

Dilute quantum liquid in a K-Rb Bose mixtureV. Cikojević^{1,2}, E. Poli,^{3,4} F. Ancilotto,⁴ L. Vranješ-Markić¹ and J. Boronat²¹*Faculty of Science, University of Split, Ruđera Boškovića 33, 21000 Split, Croatia*²*Departament de Física, Universitat Politècnica de Catalunya, Campus Nord B4-B5, 08034 Barcelona, Spain*³*Institut für Experimentalphysik, Universität Innsbruck, 6020 Innsbruck, Austria*⁴*Dipartimento di Fisica e Astronomia “Galileo Galilei” and CNISM, Università di Padova, Via Marzolo 8, 35122 Padova, Italy*

(Received 12 July 2021; accepted 13 September 2021; published 24 September 2021)

A quantum liquid in a heterogeneous mixture of ^{41}K and ^{87}Rb atoms is studied using the diffusion Monte Carlo method and density-functional theory. The perturbative Lee-Huang-Yang term for a heterogeneous mixture is verified and it is proved to be valid only near the gas-liquid transition. Based on the equations of state of the bulk mixture, calculated with diffusion Monte Carlo, extensions to Lee-Huang-Yang corrected mean-field energy functionals are presented. Using density-functional theory, a systematic comparison between different functionals is performed, focusing on the critical atom number, surface tension, surface width, Tolman length, and compressibility. These results are given as a function of the interspecies interaction strength, within the stability domain of the liquid mixture.

DOI: [10.1103/PhysRevA.104.033319](https://doi.org/10.1103/PhysRevA.104.033319)**I. INTRODUCTION**

A new quantum state of matter has been predicted [1] and experimentally realized [2–4] recently in ultracold atomic gases, where a subtle interplay between interspecies attractive interactions and quantum fluctuations may result in the formation of self-bound ultradilute droplets. Such liquid droplets are fundamentally different from those in classical or helium fluids, where they arise instead from the interplay between the short-range repulsive and long-range attractive components of the interatomic potential [5]. The existence of self-bound ultradilute quantum droplets, made of atoms of a binary mixture of Bose-Einstein condensates, was predicted by Petrov [1] and was experimentally confirmed shortly thereafter [2,3]. These systems, whose peculiar properties are shared by other systems such as dipolar Bose gases [6–8], are characterized by ultralow densities, orders of magnitude lower than that of the prototypical quantum liquid, i.e., liquid helium. Noticeably, quantum droplets exist at temperatures that are several orders of magnitude lower than the freezing points of classical liquids.

Mean-field (MF) analysis predicts that binary mixtures of Bose-Einstein condensates become unstable against collapse when the attractive interspecies interaction overcomes the repulsive contact potential between atoms [9]. However, in the ultradilute liquid phase the mean-field collapse is avoided if beyond-mean-field first-order perturbative corrections, in the form of the Lee-Huang-Yang (LHY) energy functional [10,11], are included. This correction is repulsive in nature and thus stabilizes the system.

The formation of heteronuclear quantum droplets in an attractive bosonic mixture of ^{41}K and ^{87}Rb has been observed recently [4]. At variance with the largely studied mixture of two hyperfine states of ^{39}K , longer-lived self-bound states are

observed in the K-Rb mixture, both in free space and in optical waveguides. The K-Rb mixture has proven to be robust even when the two components are exposed to different confining potentials. Such long-lived self-bound droplets remain localized on a timescale of several tens of milliseconds, more than a factor of 10 larger than in the ^{39}K mixture [3].

The increased lifetime of this new liquid mixture not only allows for a more detailed experimental observation and characterization of isolated droplets (like, e.g., the observation of the droplet self-evaporation [12]), but will also permit the observation of more complex scenarios arising from the interactions between self-bound droplets. Moreover, the observed reduction of three-body losses allows for the realization of larger droplets. Recently, collisions between two droplets have been proposed as a useful experimental tool to investigate the dynamical properties of self-bound systems [13]. When two such droplets approach each other with a given relative velocity, they can either merge in a single droplet (coalescence) or separate into two or more droplets after the collision (bouncing or fragmentation) [14]. These different outcomes depend on whether or not the surface tension is large enough to counterbalance the kinetic energy of the colliding drops. A different phenomenology is expected for the coalescence dynamics of two droplets colliding at very low velocities, which, in analogy to previous studies on helium clusters, could be a probe of their superfluid properties. One interesting outcome of collision would be the formation of vortices or other topological structures during the merging process, as a consequence of their condensate nature. These effects are known to arise during the merging of superfluid liquid-helium nanodroplets [15].

A fruitful comparison with experiments needs accurate and reliable theoretical schemes, which have not been applied yet to the K-Rb mixture. The use of density-functional

theory (DFT), in its time-dependent version, is known to allow a quite accurate description of the dynamics of inhomogeneous superfluid systems, even at the level of the local-density approximation. Finite-range effects permit one to widen the applicability of numerical simulations by going beyond the usual mean-field theory corrected with the LHY term (MF + LHY). A most natural way to include such effects within the DFT scheme is to use density functionals built from results of first-principles quantum Monte Carlo (QMC) calculations for the homogeneous phase [16,17]. Importantly, first-principles finite- N QMC calculations in the low-density regime show good agreement with the DFT approach [18] only in the vicinity of the gas-liquid transition while, at larger densities, modifications to the MF + LHY approach are necessary [19–22].

This work is organized as follows. In Sec. II we introduce the MF + LHY functional for a K-Rb mixture and predict a range of scattering lengths which allow a self-bound state. In Sec. III we describe the diffusion Monte Carlo (DMC) methodology for obtaining the ground-state energies of the bulk mixture. We report the DMC energies obtained using the short-range and finite-range potentials in Secs. IV and V, respectively. In Sec. VI we apply the density-functional formalism to the characterization of the droplets, comparing the MF + LHY and QMC-based functionals for each quantity. Namely, we provide results for the surface tension, density profile, critical atom number, surface width, compressibility, and Tolman length for an experimentally relevant range of scattering parameters. Finally, a summary of results and conclusions is given in Sec. VII.

II. THE MFLHY EQUATION OF STATE

We consider a homogeneous heteronuclear Bose-Bose mixture with two components (with masses m_1 and m_2) in a volume V and a total number of bosons $N = N_1 + N_2$. By neglecting finite-range effects (which will be considered in Sec. III), only the s -wave scattering lengths are used to characterize the interparticle interactions. Within the LHY-extended mean-field framework (abbreviated MF + LHY hereafter), the energy of the system per unit volume is given by the functional [1]

$$\mathcal{E} = \mathcal{E}_{\text{MF}} + \mathcal{E}_{\text{LHY}}, \quad (1)$$

where the mean-field and Lee-Huang-Yang terms read [9,23,24]

$$\mathcal{E}_{\text{MF}} = \frac{1}{2}g_{11}\rho_1^2 + \frac{1}{2}g_{22}\rho_2^2 + g_{12}\rho_1\rho_2, \quad (2)$$

$$\mathcal{E}_{\text{LHY}} = \frac{8m_1^{3/2}(g_{11}\rho_1)^{5/2}}{15\pi^2\hbar^3} \left[1 + \left(\frac{m_2}{m_1} \right)^{3/5} \frac{g_{22}\rho_2}{g_{11}\rho_1} \right]^{5/2}. \quad (3)$$

Here ρ_i ($i = 1, 2$) are the number densities of each component of the mixture, normalized such that $\int_V \rho_i d\mathbf{r} = N_i$, and $g_{ij} = 2\pi\hbar^2 a_{ij}/\mu_{ij}$ are the ij -interaction strengths, with $\mu_{ij}^{-1} = m_i^{-1} + m_j^{-1}$ the reduced mass.

The mixture of the two species is stable against fluctuations in the concentration N_1/N_2 if [1]

$$\frac{\rho_2}{\rho_1} = \sqrt{\frac{g_{11}}{g_{22}}}. \quad (4)$$

As pointed out in Refs. [1,23,25], it is safe to assume that this optimal composition is realized everywhere in the system. Thus, the energy functional $\mathcal{E}_{\text{MF+LHY}}[\rho] = \mathcal{E}_{\text{MF}}[\rho] + \mathcal{E}_{\text{LHY}}[\rho]$ becomes effectively a single component and can be written in terms of the total density $\rho = \rho_1 + \rho_2$. Under this assumption, the MF and LHY terms read

$$\mathcal{E}_{\text{MF}} = \frac{2\pi\hbar^2(2a_{11}m_2 + a_{12}\sqrt{\frac{a_{11}m_2}{a_{22}m_1}}(m_1 + m_2))}{m_1m_2\left(\sqrt{\frac{a_{11}m_2}{a_{22}m_1}} + 1\right)^2} \rho^2, \quad (5)$$

$$\mathcal{E}_{\text{LHY}} = \frac{256\sqrt{\pi}\hbar^2 a_{11}^{5/2}}{15m_1} \left[\frac{1 + \left(\frac{m_2}{m_1}\right)^{1/10} \sqrt{\frac{a_{22}}{a_{11}}}}{1 + \sqrt{\frac{m_2 a_{11}}{m_1 a_{22}}}} \right]^{5/2} \rho^{5/2}. \quad (6)$$

The MF + LHY energy per particle can be compactly written as

$$\frac{E/N}{|E_0^{\text{MF+LHY}}|/N} = -3 \frac{\rho}{\rho_0^{\text{MF+LHY}}} + 2 \left(\frac{\rho}{\rho_0^{\text{MF+LHY}}} \right)^{3/2}, \quad (7)$$

$\rho_0^{\text{MF+LHY}}$ being the equilibrium density within the MF + LHY theory, i.e., the density that minimizes the functional $\mathcal{E}_{\text{MF+LHY}}[\rho]$. Explicitly,

$$\rho_0^{\text{MF+LHY}} = \frac{25\pi m_2^3(2a_{11}m_2 + a_{12}\sqrt{\frac{a_{11}m_2}{a_{22}m_1}}(m_1 + m_2))^2}{4096(a_{11}m_2 + a_{22}m_1\left(\frac{m_2}{m_1}\right)^{3/5}\sqrt{\frac{a_{11}m_2}{a_{22}m_1}})^5} \times \left(\sqrt{\frac{a_{11}m_2}{a_{22}m_1}} + 1 \right). \quad (8)$$

The energy per particle at equilibrium is $E_0^{\text{MF+LHY}}/N = \mathcal{E}_{\text{MF+LHY}}[\rho_0^{\text{MF+LHY}}]/\rho_0^{\text{MF+LHY}}$. The fact that the MF + LHY functional can be written in a universal form (7) proves that all the results from Ref. [1] can be applied here with a proper change of units.

In what follows, we define the hyperfine state $|F = 1, m_F = 1\rangle$ of ^{41}K as component 1 and the hyperfine state $|F = 1, m_F = 1\rangle$ of ^{87}Rb as component 2. The scattering parameters describing the intraspecies repulsion are fixed and their values are equal to $a_{11} = 65a_0$ [26] and $a_{22} = 100.4a_0$ [27]. Notice that a slightly different value for the K-K scattering length, $a_{11} = 63a_0$, has been used more recently in Ref. [12]. With those two parameters, the MF + LHY theory predicts a self-bound state (hereafter called liquid) for $a_{12} < a_{12}^c$, with a_{12}^c given by

$$a_{12}^c = \frac{-2\sqrt{a_{22}/a_{11}}}{\sqrt{m_2/m_1}(1 + m_1/m_2)} \approx -75.4a_0. \quad (9)$$

In the experiment, accessible values of a_{12} are in the range between $a_{12} = -80a_0$ and $a_{12} = -95a_0$ [4].

III. DIFFUSION MONTE CARLO

We use the DMC method to determine the energy per particle in the homogeneous phase. This method was previ-

ously applied in related problems regarding the study of a Bose-Bose liquid by some of the authors [16,28]. Diffusion Monte Carlo is nowadays a well-know method that is able to solve exactly the imaginary-time Schrödinger equation of the many-particle system, within some statistical noise. The starting point of DMC is the decomposition of the imaginary-time evolution operator. In this paper we use a propagator that is accurate up to second order in the time step [29], following the implementation outlined in Ref. [30].

To reduce the variance in the estimation of energy, we use standard importance sampling through a trial wave function, written as a Jastrow product over pairs [31]

$$\Psi(\mathbf{R}) = \prod_{j>i=0}^{N_1} f^{(11)}(r_{ij}) \prod_{j>i=N_1}^{N_1+N_2} f^{(22)}(r_{ij}) \prod_{i,j} f^{(12)}(r_{ij}), \quad (10)$$

where the two-particle correlation functions $f^{(\alpha,\beta)}(r)$ ($\alpha, \beta = 1, 2$) are chosen as

$$f^{(\alpha,\beta)}(r) = \begin{cases} f_{2b}(r), & r < \tilde{R} \\ B(1 - \frac{a_{\alpha,\beta}}{r}), & r < R_v \\ C \exp(-\frac{D}{r} + \frac{E}{r^2}), & R_v < r < \frac{L}{2} \\ 1, & r > \frac{L}{2}. \end{cases} \quad (11)$$

The two-particle correlation function at short distances $f_{2b}(r)$ is the solution to the two-body problem for a given interaction potential. Throughout the paper we use short-range potentials such that the potential is zero at distances greater than \tilde{R} . The function f_{2b} is connected to the asymptotic form $1 - a_{\alpha,\beta}/r$, where $a_{\alpha,\beta}$ is a corresponding scattering length. At $r = R_v$, this is connected to the long-range phononic form $C \exp(-\frac{D}{r} + \frac{E}{r^2})$ [32]. Finally, we impose that the function is constant (one) at the boundary of the simulation box ($r = L/2$). This trial wave function has only one variational parameter, namely, R_v , which we optimize variationally finding that, in all cases, $R_v = 0.45L$. Our DMC results are unbiased for time steps $\Delta\tau \lesssim 0.5m_4a_{11}^2/\hbar^2$ and walker number $n_w \approx 200$. Simulations are performed in a cubic box of size $L = (N/\rho)^{1/3}$, with periodic boundary conditions applied to particle coordinates. For each density, a set of several calculations of increasing number of particles, namely, $N = 130, 160, 200, 250, \text{ and } 500$, is performed in order to study finite-size effects. The final energies, corresponding to the thermodynamic limit, are obtained by an extrapolation to $N \rightarrow \infty$ assuming a correction which decreases as N^{-1} .

IV. SHORT-RANGE POTENTIALS

In a first approach to the problem, we use in DMC interatomic potentials that have a very short range, which we call SRPOTs in the following. Since we cannot use a contact interaction in DMC, we model the short-range interaction by a set of potentials with a range r_p satisfying $\rho r_p^3 \ll 1$, where ρ is the typical number density. Under this criterion, we choose a hard-core potential for repulsive interactions (between equal species), with a diameter corresponding to the s -wave scattering length [9]

$$V_{ii}(r) = \begin{cases} \infty & \text{for } r < a_{ii}, \quad i = 1, 2 \\ 0 & \text{otherwise.} \end{cases} \quad (12)$$

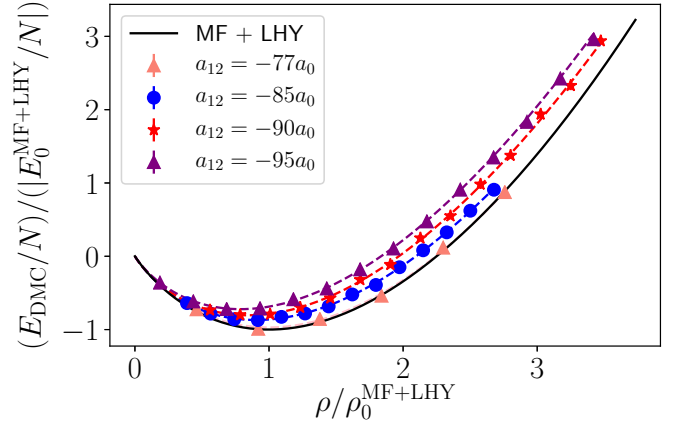


FIG. 1. Diffusion Monte Carlo energy per particle as a function of density, obtained with the SRPOT models [Eqs. (12) and (13)], in a mixture having the optimal composition $\rho_2/\rho_1 = \sqrt{g_{11}/g_{22}}$. The energy per particle and the total density are normalized with respect to the equilibrium values given in Eq. (8).

The attraction between different species is modeled by a short-range square-well potential

$$V_{12}(r) = \begin{cases} -V_{\text{sr}} & \text{for } r < R_{\text{sr}} \\ 0 & \text{otherwise,} \end{cases} \quad (13)$$

where we choose $R_{\text{sr}} = a_{11}$. The particular choice of potentials given in Eqs. (12) and (13) resembles a zero-range case, since the probability of finding two particles within the diameter R_{sr} is $\rho_0 R_{\text{sr}}^3 \approx 2 \times 10^{-4}$, evaluated at the equilibrium density for the densest liquid analyzed, corresponding to $a_{12} = -95a_0$. By properly setting V_{sr} , we obtain a target scattering length a_{12} , which for a square-well potential is given by [33]

$$a_{12} = R_{\text{sr}} \left\{ 1 + \frac{\tan(K_0 R_{\text{sr}})}{K_0 R_{\text{sr}}} \right\}, \quad (14)$$

where $K_0 = \sqrt{2V_{\text{sr}}(m_1 + m_2)/\hbar^2 m_1 m_2}$. The DMC results of the energy per particle, obtained with SRPOTs (12) and (13), are shown in Fig. 1 for $a_{12} = -77a_0, -85a_0, -90a_0, \text{ and } -95a_0$, which include experimentally accessible values. They are compared with the predictions of MF + LHY theory. The DMC energy per particle is well fitted to the form

$$\frac{E}{N} = \alpha\rho + \beta\rho^\gamma, \quad (15)$$

where α, β , and γ are the fitting parameters. The equilibrium density and the coefficients of the fit to the DMC energy per particle are reported in Table I. As we can see in Fig. 1, the DMC results of the energy per particle reproduce well the MF + LHY theory for $a_{12} = -77a_0$, which is close to the critical value $a_{12}^c = -75.4a_0$. However, the DMC results for different a_{12} do not fit a single line defined by Eq. (7), implying that the universality of the MF + LHY theory is broken, with the deviation growing as a_{12} becomes larger. Interestingly, we observe repulsive beyond-LHY contributions when the fluid enters a more correlated regime. Repulsive beyond-LHY contributions to the energy have already been observed in symmetric Bose-Bose fluids [28] and in the liquid

TABLE I. Coefficients of fit $E/N = \alpha \rho a_{11}^3 + \beta (\rho a_{11}^3)^\gamma$ of the DMC energies per particle, obtained with a short-range set of potentials [Eqs. (12) and (13), reported in Fig. 1]. The parameters α and β are given in units of $\hbar^2/m_1 a_{11}^2 = 10^{-3}$ K and γ is adimensional. Here ρ_0 stands for the equilibrium density of a QMC functional. Scattering lengths in the repulsive channel are $a_{11} = 65a_0$ and $a_{22} = 100.4a_0$.

a_{12}	Method	α	β	γ	$\rho_0 a_{11}^3$
$-77a_0$	QMC	-0.056	35.709	1.500	1.08×10^{-6}
$-77a_0$	MF+LHY	-0.057	36.437	1.5	1.09×10^{-6}
$-85a_0$	QMC	-0.385	15.981	1.395	3.48×10^{-5}
$-85a_0$	MF+LHY	-0.340	36.437	1.5	3.86×10^{-5}
$-90a_0$	QMC	-0.592	16.344	1.384	7.53×10^{-5}
$-90a_0$	MF+LHY	-0.516	36.437	1.5	8.92×10^{-4}
$-95a_0$	QMC	-0.772	16.768	1.379	1.26×10^{-4}
$-95a_0$	MF+LHY	-0.693	36.437	1.5	1.61×10^{-4}

^{39}K mixture [16] for the potentials with a small effective range. This effect could be due to bosonic pairing between atoms of different species [20,21].

V. FINITE-RANGE POTENTIALS

The effective range in the ^{41}K - ^{87}Rb mixture is not known, but can be estimated from the combined knowledge of the C_6 coefficient of the leading term in the long-range tail of the van der Waals interaction potential and the scattering length obtained from measurements of the Feshbach resonances [34–36]. Knowing the van der Waals coefficient C_6 , one can estimate the effective range using a semiclassical approximation [36]

$$r_{\text{eff}} = \frac{\Gamma(\frac{1}{4})^2}{6\pi} a_m \left[1 - 2\frac{a_m}{a} + 2\left(\frac{a_m}{a}\right)^2 \right], \quad (16)$$

with $a_m = 4\pi R_{\text{vdW}}/\Gamma(\frac{1}{4})^2$ the mean scattering length and $R_{\text{vdW}} = (2\mu C_6/\hbar^2)^{1/4}/2$ the van der Waals length, where μ is the reduced mass. The C_6 coefficients for ^{41}K and ^{87}Rb are given, along with the effective ranges derived from (16), in Table II.

Since only two scattering parameters, namely, the scattering length a and the effective range r_{eff} , cannot uniquely define the interaction potential, we resort to model potentials satisfying the two scattering criteria. To investigate the role of the shape of the interaction dictated by the higher-order

TABLE II. Coefficients C_6 of each channel and the corresponding scattering lengths and effective ranges.

Channel	C_6 (a.u.)	a/a_0	r_{eff}/a_0
K-K (1-1) ^a	3897	65	168
Rb-Rb (2-2) ^b	4707	100.4	153
K-Rb (1-2) ^c	4285	-85	795
		-90	748
		-95	707

^aReferences [26,37].

^bReference [27].

^cReference [38].

TABLE III. Parameters of potentials POT-I and POT-II which reproduce both scattering parameters (see Table II). Here R_0 and R_1 are given in units of $a_{11} = 65a_0$, and V_0 and V_1 are given in units of $\hbar^2/m_1 a_{11}^2 = 10^{-3}$ K.

a	Potential	R_0	R_1	V_0	V_1
$65a_0$	POT-I	1.8797	0	1.2123	0
$65a_0$	POT-II	2.8386	3.5581	0.9140	0.3687
$100.4a_0$	POT-I	2.7084	0	0.3337	0
$100.4a_0$	POT-II	3.8374	4.8201	0.2366	0.0824
$-85a_0$	POT-I	0	4.8897	0	0.01865
$-85a_0$	POT-II	2.7513	3.6684	0.0632	0.1189
$-90a_0$	POT-I	0	4.8069	0	0.0205
$-90a_0$	POT-II	2.7419	3.6558	0.0586	0.1197
$-95a_0$	POT-I	0	4.7315	0	0.0222
$-95a_0$	POT-II	2.7329	3.6438	0.0541	0.1205

scattering parameters, we performed two independent sets of calculations, each having different models of the interaction potential. We call the two models POT-I and POT-II and both can be written as

$$V(r) = \begin{cases} V_0 & \text{for } 0 < r < R_0 \\ -V_1 & \text{for } R_0 < r < R_1, \quad i = 1, 2 \\ 0 & \text{otherwise.} \end{cases} \quad (17)$$

This particular form of interaction is convenient because the analytic expressions for both the s -wave scattering length and effective range are analytically known [39]. The specific values of the interaction parameters in all three channels for potentials POT-I and POT-II are summarized in Table III.

In Fig. 2 we report the comparison between the DMC and MF + LHY equations of state for three values of a_{12} and using POT-I and POT-II as model potentials (see Table IV). For all three values of a_{12} , there is a slight increase in the equilibrium density, relative to the MF + LHY theory. This phenomenon was previously observed in a mixture with symmetric interactions [18,19,28], whereas in a ^{39}K liquid mixture [16] the significant increase of equilibrium density occurs because in that mixture the effective range is much larger than in the K-Rb one. In other words, in the K mixture the finite-range, beyond-LHY, negative energy contributions dominate. On the

TABLE IV. Coefficients of fit $E/N = \alpha \rho a_{11}^3 + \beta (\rho a_{11}^3)^\gamma$ of the DMC energy per particle, obtained with a set of potentials POT-I and POT-II [see Eq. (17) and Table III]. (A comparison of different functionals is presented in Fig. 2.) The parameters α and β are given in units of $\hbar^2/m_1 a_{11}^2 = 10^{-3}$ K and γ is adimensional. Scattering lengths in the repulsive channel are $a_{11} = 65a_0$ and $a_{22} = 100.4a_0$. For comparison, the MF+LHY parameters are given in Table I.

a_{12}	Potentials	α	β	γ
-85	POT-I	-0.37	14.087	1.393
-85	POT-II	-0.371	14.547	1.396
-90	POT-I	-0.578	11.778	1.359
-90	POT-II	-0.573	12.894	1.369
-95	POT-I	-0.824	9.752	1.316
-95	POT-II	-0.774	12.22	1.351

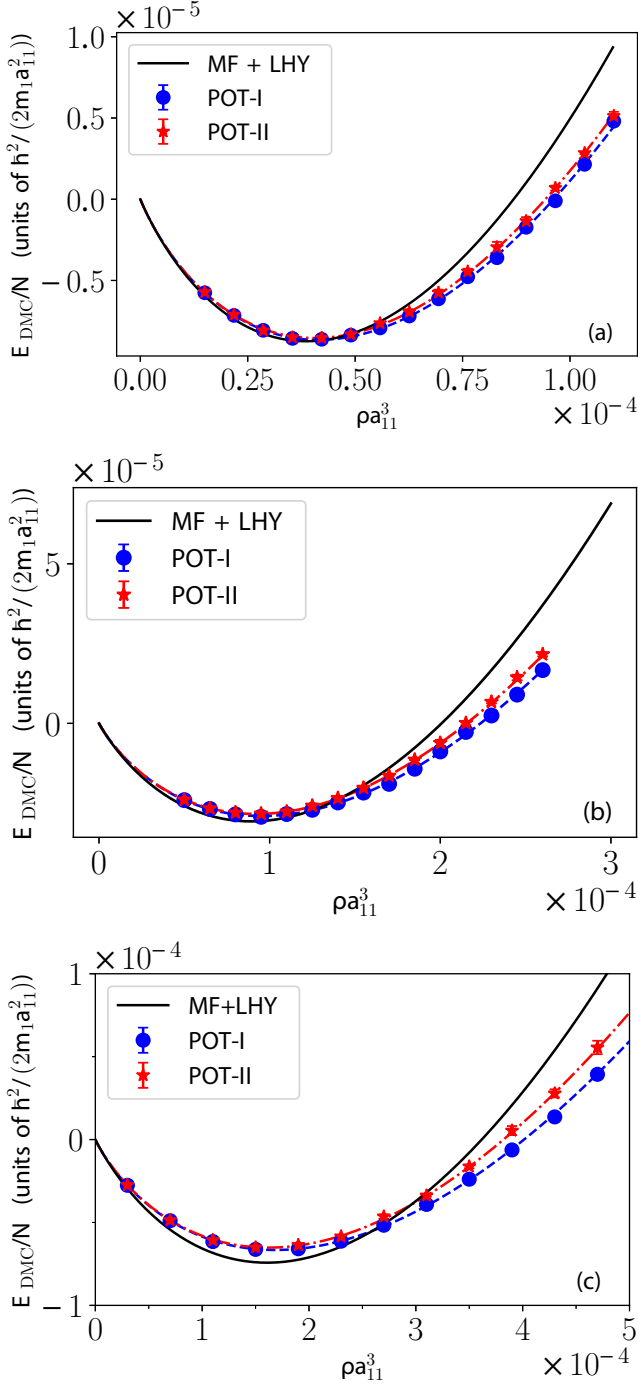


FIG. 2. Energy per particle as a function of density, for values of (a) $a_{12} = -85a_0$, (b) $a_{12} = -90a_0$, and (c) $a_{12} = -95a_0$. The DMC calculations are performed with potentials POT-I and POT-II, which satisfy both scattering parameters [see Eq. (17) and Table IV]. The ratio of concentrations $\rho_2/\rho_1 = \sqrt{g_{11}/g_{22}}$ is kept fixed for each density, a criterion coming from the mean field, also verified by QMC to predict the ground state.

other hand, we observe that energies obtained with two different potentials but with the same s -wave scattering length and effective range collapse to a single equation of state, at least at densities not much larger than the equilibrium one. Therefore,

the range of universality is extended, but now in terms of two scattering parameters [16].

VI. DENSITY-FUNCTIONAL RESULTS

The stability of the self-bound mixture of $^{41}\text{K} - ^{87}\text{Rb}$ in free space implies the presence of a surface and a positive surface tension associated with it. We studied the surface properties of spherical $^{41}\text{K} - ^{87}\text{Rb}$ droplets within the DFT approach in the MF + LHY framework, for a fixed ratio of densities $\rho_2/\rho_1 = \sqrt{g_{11}/g_{22}}$ corresponding to the equilibrium one for the homogeneous mixture. We provide additional results using a more accurate density functional obtained from the *ab initio* QMC results discussed in the preceding section.

We first studied a planar surface, with the aim of determining the surface tension σ in a range of values of the interparticle attractive interaction a_{12} accessible to the experiments. When studying a planar surface, it is useful to use a slab geometry, i.e., we assume an extended homogeneous system in the xy plane (with periodic boundary conditions) and with a finite extension in the z direction. In this direction, two liquid-vacuum interfaces are formed, with the slab width thick enough to have a constant density region between the two confining surfaces (bulk phase). This amounts to neglecting curvature effects, which will be explicitly considered later on. The surface width of the density profile along z can be quantified by the parameter Δ , which measures the width between surface points at 90% and 10% of the bulk total density.

By defining the coefficients

$$C_K = \frac{1}{4} \left(\frac{\hbar^2}{2m_1} + \frac{\hbar^2}{2m_2} \sqrt{\frac{g_{11}}{g_{22}}} \right), \quad (18)$$

$$C_\delta = g_{11} + g_{12} \sqrt{\frac{g_{11}}{g_{22}}}, \quad (19)$$

$$C_\rho = \frac{8}{15\pi^2} \left(\frac{m_1}{\hbar^2} \right)^{3/2} g_{11}^{5/2} \left[1 + \left(\frac{m_1}{m_2} \right)^{3/5} \sqrt{\frac{g_{22}}{g_{11}}} \right], \quad (20)$$

the effective single-component energy density of the mixture within the MF + LHY theory, expressed for simplicity in terms of the density ρ_1 , reads

$$\mathcal{E} = C_K \frac{(\nabla \rho_1)^2}{\rho_1} + C_\delta \rho_1^2 + C_\rho \rho_1^{5/2}. \quad (21)$$

We recall that knowledge of one density is enough to characterize the whole droplet because of the underlying assumption $\rho_2/\rho_1 = \sqrt{g_{11}/g_{22}}$ [23,25].

Remarkably, the surface tension of the planar interface described by local energy functionals of the form (21) can be estimated, without any prior knowledge of the density profile, by calculating the integral [40]

$$\sigma = 2 \int_0^{\rho_0} d\rho_1 \sqrt{C_K (C_\delta \rho_1 + C_\rho \rho_1^{3/2} - \mu_0)}, \quad (22)$$

where $\mu_0 = C_\delta \rho_1 + C_\rho \rho_1^{3/2}$ is the chemical potential of a liquid system in equilibrium with the vacuum, evaluated at the equilibrium density ρ_0 . The density profile can also be

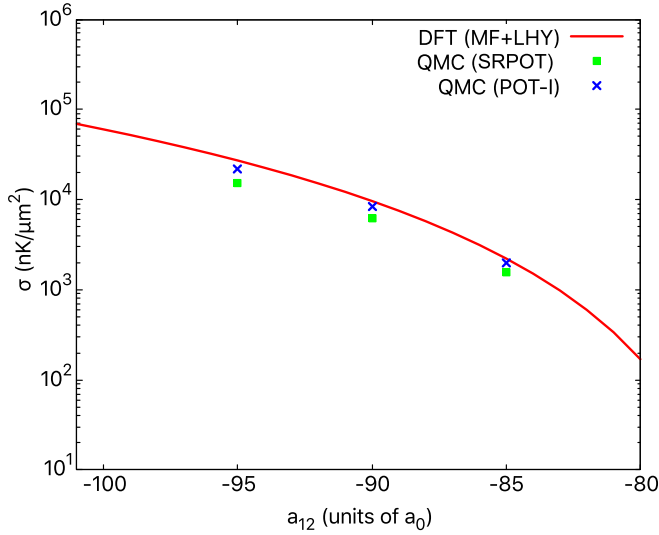


FIG. 3. Surface tension as a function of the (attractive) interspecies scattering length a_{12} . The red solid line is obtained using the MF + LHY functional; green squares and blue crosses are the predictions assuming SRPOT and POT-I functionals, respectively (see Tables I and IV).

obtained by simple quadrature, solving the implicit equation

$$z(\rho) = z_0 + \int_{\rho_0/2}^{\rho} \frac{1}{h(\rho')} d\rho', \quad (23)$$

where $\rho(z_0) = \rho_0/2$ and

$$h(\rho) = -\sqrt{\left(\frac{\rho}{C_K}\right)[C_\delta \rho^2 + C_\rho \rho^{5/2} - \mu_0 \rho]}. \quad (24)$$

Here ρ can have any value in the interval $[0, \rho_0]$.

The calculated surface tension for different values of a_{12} is shown in Fig. 3 and compared with the results obtained from the QMC-based functional. Notice that relatively small changes in the interspecies interaction strength cause order-of-magnitude changes in the surface tension, which is highlighted by the logarithmic scale introduced on the σ axis. Surface tension obtained with the QMC-based functionals SRPOT and POT-I are both below the predictions of the MF + LHY functional, with SRPOT having larger deviations from MF + LHY.

The width of the liquid-vacuum interface profile is strongly dependent on the interspecies scattering length a_{12} . In a droplet this will affect the overall shape of the droplet itself, depending upon the value of the total number of particles N . For larger values of N the droplet will be characterized by a central region of fairly uniform density (bulk) and an external surface region where the density drops to zero with the distance from its center, whereas it will be an all-surface Gaussian-like droplet, where the central bulk region is almost absent, for low values of N . By defining the droplet radius R as

$$R = \sqrt[3]{\frac{3N}{4\pi \rho_{\text{bulk}}}}, \quad (25)$$

in the first case the ratio between the surface width Δ and the droplet radius R is $\Delta/R \ll 1$, while in the second case $\Delta/R \gg 1$.

We must notice that not all values of N are allowed in a droplet for a given a_{12} because small droplets, i.e., those with a number of particles below some critical value N_c , become unstable when the kinetic energy dominates over the interaction energy, eventually causing the evaporation of the droplet. In order to estimate the critical size N^c we make a simple variational ansatz for the radial density profile, which is a good approximation for spherical small droplets:

$$\rho_1(r) = \frac{N_1}{\pi^{3/2} \sigma^3} e^{-r^2/\sigma^2}. \quad (26)$$

We use the above ansatz in the energy functional (21) and impose the condition for a minimum, $\partial E/\partial \sigma = 0$, together with the additional requirement $E = 0$, which marks the line separating stable droplets with negative total energies from unstable ones with positive energies. Solving for the total number of atoms of species 1, N_1 , we find the critical droplet size $N_c = N_{c1}(1 + \sqrt{g_{11}/g_{22}})$, where

$$N_{c1} = -\frac{c}{\lambda^{9/2}(a/\lambda^2 + b/\lambda^3)}, \quad (27)$$

with $\lambda = -3b/5a$. Here a , b , and c are given by the expressions $a = 6C_K$, $b = C_\delta/2\pi^{3/2}$, and $c = 4C_\rho/5\sqrt{10}\pi^{9/4}$. Table V and Fig. 4 show the critical atom number for some values of the scattering length computed with DFT and QMC methods.

Figure 5 summarizes our results. The color scale shows the ratio between the surface width Δ and the radius R of the droplet, which evaporates for a number of particles below the critical value (black solid line). The red region identifies Gaussian-like all-surface droplets, while the green and blue regions identify droplets with a well-defined central bulk density. Notice that the black line belongs to the red region for each $|a_{12}|$, so the assumption of a Gaussian density profile for the variational study of the critical atom number is indeed justified.

The surface tension for the $^{41}\text{K} - ^{87}\text{Rb}$ self-bound mixture has been obtained for a planar interface (we will call it σ_0 to distinguish it from the size-dependent surface tension of a droplet), though in real droplets an interfacial curvature of the surface in contact with the vacuum is present. The curvature-dependent surface tension can be expressed in terms of the so-called Tolman length δ [41]. To a first approximation the Tolman length δ is independent of the droplet size and it gives the size-dependent surface tension in terms of the one for a planar surface [42,43]

$$\sigma(R) = \sigma_0 \left(1 - \frac{2\delta}{R}\right). \quad (28)$$

A thermodynamic argument relates the Tolman length to the isothermal compressibility κ^{-1} and surface tension σ_0 [44],

$$\delta \approx -\kappa^{-1} \sigma_0. \quad (29)$$

The isothermal compressibility κ^{-1} of a self-bound quantum mixture with equilibrium bulk densities ρ_1 and ρ_2 in the

TABLE V. Summary of all the quantities reported in the paper. Mass m is the mass of the ^{41}Rb atom and a_0 is the Bohr radius. Here $\epsilon_r(\text{SRPOT})$ and $\epsilon_r(\text{POT-I})$ are the relative differences $(O^{\text{SRPOT}} - O^{\text{MF+LHY}})/|O^{\text{MF+LHY}}|$ and $(O^{\text{POT-I}} - O^{\text{MF+LHY}})/|O^{\text{MF+LHY}}|$ for observable O , given in percentages. Positive (negative) values of ϵ_r mean that QMC functionals predict higher (lower) values of the observable with respect to the MF+LHY one.

Observable	a_{12}/a_0	MF+LHY	SRPOT	POT-I	$\epsilon_r(\text{SRPOT})$	$\epsilon_r(\text{POT-I})$
N_c	-85	2.07×10^4	2.31×10^4	2.26×10^4	12	9
N_c	-90	7.28×10^3	8.47×10^3	8.31×10^3	16	14
N_c	-95	3.49×10^3	4.44×10^3	4.10×10^3	27	17
$\frac{\sigma}{\hbar^2/ma_0^4}$	-85	1.97×10^{-20}	1.40×10^{-20}	1.77×10^{-20}	-29	-10
$\frac{\sigma}{\hbar^2/ma_0^4}$	-90	8.55×10^{-20}	5.45×10^{-20}	7.42×10^{-20}	-36	-13
$\frac{\sigma}{\hbar^2/ma_0^4}$	-95	2.40×10^{-19}	1.34×10^{-19}	1.95×10^{-19}	-44	-19
Δ/a_0	-85	4.17×10^4	4.78×10^4	4.48×10^4	14	7
Δ/a_0	-90	2.23×10^4	2.65×10^4	2.46×10^4	19	11
Δ/a_0	-95	1.43×10^4	1.80×10^4	1.65×10^4	26	15
δ/a_0	-85	-5.53×10^3	-6.57×10^3	-6.16×10^3	-19	-11
δ/a_0	-90	-2.95×10^3	-3.67×10^3	-3.43×10^3	-24	-16
δ/a_0	-95	-1.90×10^3	-2.50×10^3	-2.35×10^3	-32	-24
$\frac{\kappa^{-1}}{ma_0^2/\hbar^2}$	-85	2.81×10^{23}	4.69×10^{23}	3.47×10^{23}	67	24
$\frac{\kappa^{-1}}{ma_0^2/\hbar^2}$	-90	3.45×10^{22}	6.73×10^{22}	4.62×10^{22}	95	34
$\frac{\kappa^{-1}}{ma_0^2/\hbar^2}$	-95	7.90×10^{21}	1.86×10^{22}	1.20×10^{22}	135	52

MF + LHY approach is given by [23]

$$\kappa^{-1} = (g_{11}\rho_1^2 + g_{22}\rho_2^2 + 2g_{12}\rho_1\rho_2 + \frac{15}{4}\mathcal{E}_{\text{LHY}})^{-1}. \quad (30)$$

Previously, some studies have noticed that the product $\kappa^{-1}\sigma_0$ is a fundamental characteristic length in liquid droplets [45–49] though the connection with the Tolman length δ was never explicitly made. We checked the validity of Eq. (29) by independently computing δ using the liquid drop model (LDM), i.e., writing the calculated total energy of a droplet made of N atoms as

$$E = a'N + b'N^{2/3} + c'N^{1/3}, \quad (31)$$

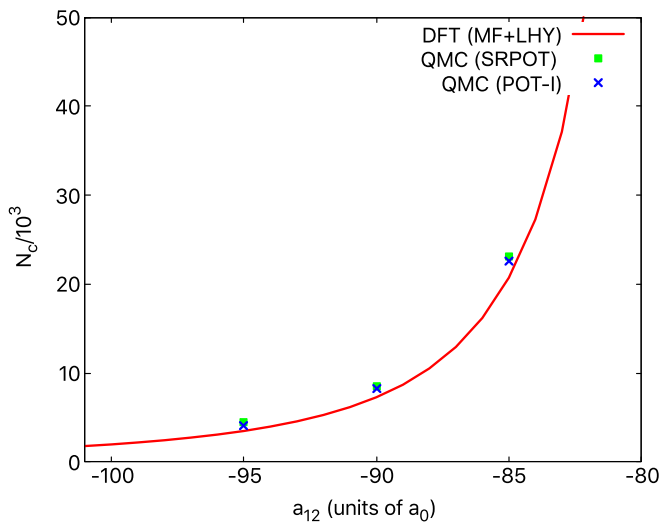


FIG. 4. Critical atom number N_c as a function of the interspecies scattering length. The red solid line is obtained using the MF + LHY functional; green squares and blue crosses are the predictions assuming SRPOT and POT-I functionals, respectively (see Tables I and IV).

where the separate bulk, surface, and curvature contributions to the total energy of the droplet are highlighted. By using the relation (28), one can see that $c' = 8\pi(3/4\pi\rho_0)^{1/3}\sigma_0\delta$. The coefficient c' is in turn obtained by fitting the calculated energies using the LDM expression quoted above, allowing one to determine the Tolman length δ . Predictions for the Tolman length are summarized in Table V.

In Fig. 6 the compressibility computed with the MF + LHY approach is shown for a set of values of the scattering length and compared to QMC results. In contrast to ^{39}K

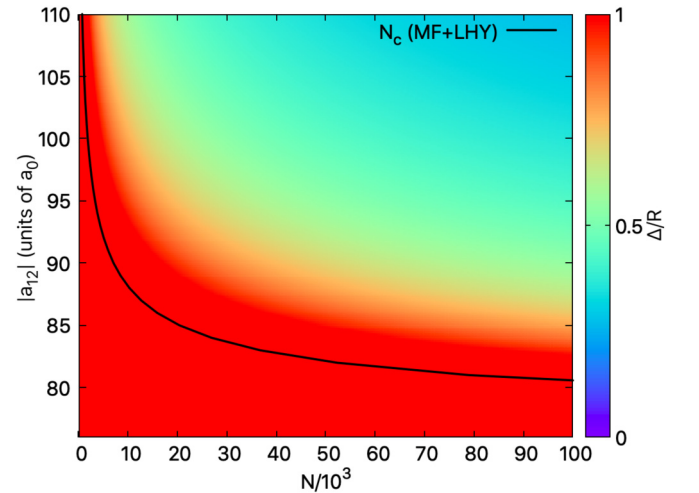


FIG. 5. Ratio Δ/R represented as a function of $|a_{12}|$ and N . The red region (darker region in the lower part of the figure) identifies Gaussian-like radial density profiles, while the green region (lighter portion in the middle) and blue region (lighter portion in the upper part) identify droplets with a central bulk region. The black solid line marks the total critical number of particles N_c below which the droplet evaporates.

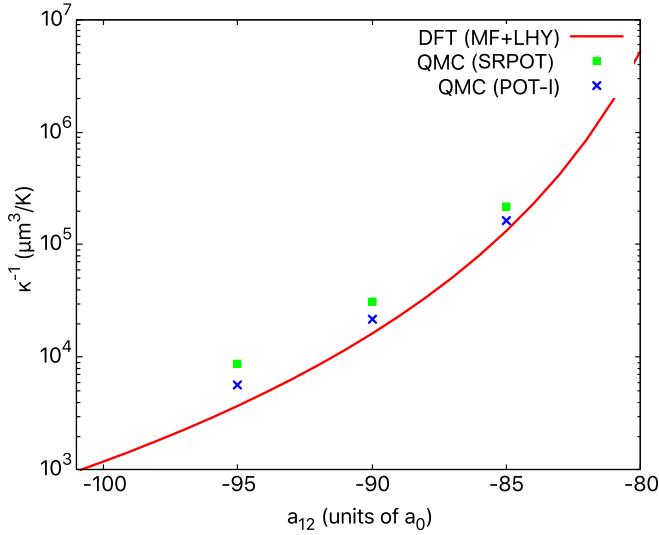


FIG. 6. Compressibility κ^{-1} as a function of the interspecies scattering length a_{12} in the self-bound droplet regime. The red solid line is obtained using the MF + LHY functional; green squares and blue crosses are the predictions assuming SRPOT and POT-I functionals, respectively (see Tables I and IV).

droplets [17], the compressibility of the QMC-based functional is higher compared to that of the MF + LHY, due to relatively smaller values of effective ranges in a K-Rb mixture.

Figure 7 shows the calculated radial density profile for a droplet with $a_{12} = -90a_0$, where a comparison is made between the prediction of the MF + LHY approach and those from the QMC-based energy functionals. The QMC-based functional, which relies on short-range model potentials (see Fig. 1), predicts less dense droplets due to repulsive beyond-LHY energy contributions. Profiles obtained with the POT-I

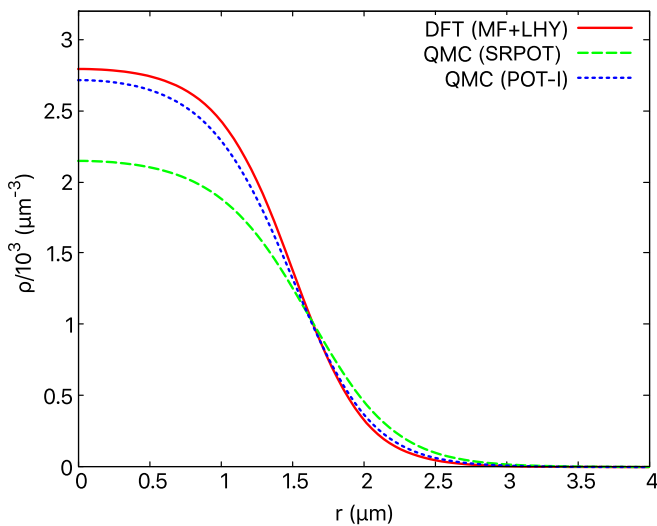


FIG. 7. Radial density profile for a droplet with $a_{12} = -90a_0$. The prediction of MF + LHY (red solid line) is compared with the results obtained from a density functional reproducing the QMC results, at zero range (SRPOT, green dashed line) and with finite-range effects (POT-I, blue dashed line).

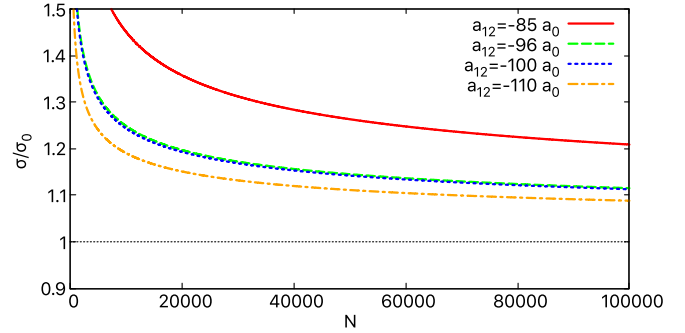


FIG. 8. Corrected and normalized surface tension σ/σ_0 as a function of the total number of particles N in the droplet for a set of values of the interspecies scattering length a_{12} , computed within the MF + LHY framework.

and MF + LHY functionals are more similar since the effect of increasing the effective range, included in POT-I through model potentials, is to increase binding energy and the peak density.

In Fig. 8 we show the dependence of the corrected surface tension σ as a function of the droplet's total number of particles N , computed within the MF + LHY framework by combining Eq. (28) with Eq. (25).

In Table V we summarize the predictions for all observables analyzed in our work with the MF + LHY and QMC-based functionals for $a_{12} = -85a_0, -90a_0,$ and $-95a_0$. It can be seen that QMC functionals show increasing deviation from the predictions of the MF + LHY functional as $|a_{12}|$ increases. Quantum Monte Carlo-based density functionals constructed assuming short-range model potentials predict larger deviations from the MF + LHY theory. When the correct effective range is included in the model potentials (POT-I), the predictions become more similar to those of MF + LHY. The variable most sensitive to beyond-LHY energy corrections appears to be the compressibility κ^{-1} , with a relative difference in the range from approximately 20% to 130%. This could have an impact on the collective excitation modes of a droplet [50], which are left for future study.

VII. CONCLUSION

We have performed QMC calculations for the ground state of a K-Rb liquid mixture. We found that the zero-range model potentials used in a QMC calculation predict significant beyond-LHY energy contributions. Otherwise, when the s -wave effective range is included in the model potentials, the energies fall close to the MF + LHY energies. Using both the MF + LHY and the QMC-based functionals, we have investigated fundamental surface properties for an experimentally relevant range of scattering parameters. These properties are relevant to the ongoing experiments because the observed droplets have a large surface-to-volume ratio. Upon entering a more correlated (denser) regime, the differences between the predictions for all quantities with the MF + LHY and the QMC-based functional grow.

ACKNOWLEDGMENTS

This work was supported by the Ministerio de Economía, Industria y Competitividad (Spain) through Grants No. FIS2017-84114-C2-1-P and No. FIS2017-87801-P (AEI/FEDER, UE) and by the EC Research Innovation Action under the H2020 Programme, Project HPC-EUROPA3 (No. INFRAIA-2016-1-730897). V.C. gratefully

acknowledges the computer resources and technical support provided by Barcelona Supercomputing Center. We also acknowledge financial support from Secretaria d'Universitats i Recerca del Departament d'Empresa i Coneixement de la Generalitat de Catalunya, cofunded by the European Union Regional Development Fund within the ERDF Operational Program of Catalunya (Project QuantumCat, No. 001-P-001644).

-
- [1] D. S. Petrov, Quantum Mechanical Stabilization of a Collapsing Bose-Bose Mixture, *Phys. Rev. Lett.* **115**, 155302 (2015).
- [2] C. Cabrera, L. Tanzi, J. Sanz, B. Naylor, P. Thomas, P. Cheiney, and L. Tarruell, Quantum liquid droplets in a mixture of Bose-Einstein condensates, *Science* **359**, 301 (2018).
- [3] G. Semeghini, G. Ferioli, L. Masi, C. Mazzinghi, L. Wolswijk, F. Minardi, M. Modugno, G. Modugno, M. Inguscio, and M. Fattori, Self-Bound Quantum Droplets of Atomic Mixtures in Free Space, *Phys. Rev. Lett.* **120**, 235301 (2018).
- [4] C. D'Errico, A. Burchianti, M. Prevedelli, L. Salasnich, F. Ancilotto, M. Modugno, F. Minardi, and C. Fort, Observation of quantum droplets in a heteronuclear bosonic mixture, *Phys. Rev. Research* **1**, 033155 (2019).
- [5] M. Barranco, R. Guardiola, S. Hernández, R. Mayol, J. Navarro, and M. Pi, Helium nanodroplets: An overview, *J. Low Temp. Phys.* **142**, 1 (2006).
- [6] F. Böttcher, M. Wenzel, J.-N. Schmidt, M. Guo, T. Langen, I. Ferrier-Barbut, T. Pfau, R. Bombín, J. Sánchez-Baena, J. Boronat, and F. Mazzanti, Dilute dipolar quantum droplets beyond the extended Gross-Pitaevskii equation, *Phys. Rev. Research* **1**, 033088 (2019).
- [7] L. Chomaz, S. Baier, D. Petter, M. J. Mark, F. Wächtler, L. Santos, and F. Ferlaino, Quantum-Fluctuation-Driven Crossover from a Dilute Bose-Einstein Condensate to a Macrodroplet in a Dipolar Quantum Fluid, *Phys. Rev. X* **6**, 041039 (2016).
- [8] R. N. Bisset, L. A. P. Ardila, and L. Santos, Quantum Droplets of Dipolar Mixtures, *Phys. Rev. Lett.* **126**, 025301 (2021).
- [9] C. J. Pethick and H. Smith, *Bose-Einstein Condensation in Dilute Gases* (Cambridge University Press, Cambridge, 2008).
- [10] T. D. Lee, K. Huang, and C. N. Yang, Eigenvalues and eigenfunctions of a Bose system of hard spheres and its low-temperature properties, *Phys. Rev.* **106**, 1135 (1957).
- [11] D. M. Larsen, Binary mixtures of dilute Bose gases with repulsive interactions at low temperature, *Ann. Phys. (NY)* **24**, 89 (1963).
- [12] C. Fort and M. Modugno, Self-evaporation dynamics of quantum droplets in a ^{41}K - ^{87}Rb mixture, *Appl. Sci.* **11**, 866 (2021).
- [13] G. Ferioli, G. Semeghini, L. Masi, G. Giusti, G. Modugno, M. Inguscio, A. Galemí, A. Recati, and M. Fattori, Collisions of Self-Bound Quantum Droplets, *Phys. Rev. Lett.* **122**, 090401 (2019).
- [14] V. Cikojević, L. V. Markić, M. Pi, M. Barranco, F. Ancilotto, and J. Boronat, Dynamics of equilibration and collisions in ultradilute quantum droplets, [arXiv:2104.09102](https://arxiv.org/abs/2104.09102).
- [15] J. M. Escartín, F. Ancilotto, M. Barranco, and M. Pi, Vorticity and quantum turbulence in the merging of superfluid helium nanodroplets, *Phys. Rev. B* **99**, 140505(R) (2019).
- [16] V. Cikojević, L. V. Markić, and J. Boronat, Finite-range effects in ultradilute quantum drops, *New J. Phys.* **22**, 053045 (2020).
- [17] V. Cikojević, L. V. Markić, M. Pi, M. Barranco, and J. Boronat, Towards a quantum Monte Carlo-based density functional including finite-range effects: Excitation modes of a ^{39}K quantum droplet, *Phys. Rev. A* **102**, 033335 (2020).
- [18] L. Parisi and S. Giorgini, Quantum droplets in one-dimensional Bose mixtures: A quantum Monte Carlo study, *Phys. Rev. A* **102**, 023318 (2020).
- [19] D. S. Petrov and G. E. Astrakharchik, Ultradilute Low-Dimensional Liquids, *Phys. Rev. Lett.* **117**, 100401 (2016).
- [20] M. Ota and G. E. Astrakharchik, Beyond Lee-Huang-Yang description of self-bound Bose mixtures, *SciPost Phys.* **9**, 20 (2020).
- [21] H. Hu and X.-J. Liu, Consistent Theory of Self-Bound Quantum Droplets with Bosonic Pairing, *Phys. Rev. Lett.* **125**, 195302 (2020).
- [22] V. Cikojević, K. Dželalija, P. Stipanović, L. Vranješ Markić, and J. Boronat, Ultradilute quantum liquid drops, *Phys. Rev. B* **97**, 140502(R) (2018).
- [23] F. Ancilotto, M. Barranco, M. Guilleumas, and M. Pi, Self-bound ultradilute Bose mixtures within local density approximation, *Phys. Rev. A* **98**, 053623 (2018).
- [24] F. Minardi, F. Ancilotto, A. Burchianti, C. D'Errico, C. Fort, and M. Modugno, Effective expression of the Lee-Huang-Yang energy functional for heteronuclear mixtures, *Phys. Rev. A* **100**, 063636 (2019).
- [25] C. Staudinger, F. Mazzanti, and R. E. Zillich, Self-bound Bose mixtures, *Phys. Rev. A* **98**, 023633 (2018).
- [26] C. D'Errico, M. Zaccanti, M. Fattori, G. Roati, M. Inguscio, G. Modugno, and A. Simoni, Feshbach resonances in ultracold ^{39}K , *New J. Phys.* **9**, 223 (2007).
- [27] A. Marte, T. Volz, J. Schuster, S. Dürr, G. Rempe, E. G. M. van Kempen, and B. J. Verhaar, Feshbach Resonances in Rubidium 87: Precision Measurement and Analysis, *Phys. Rev. Lett.* **89**, 283202 (2002).
- [28] V. Cikojević, L. V. Markić, G. E. Astrakharchik, and J. Boronat, Universality in ultradilute liquid Bose-Bose mixtures, *Phys. Rev. A* **99**, 023618 (2019).
- [29] A. Sarsa, J. Boronat, and J. Casulleras, Quadratic diffusion Monte Carlo and pure estimators for atoms, *J. Chem. Phys.* **116**, 5956 (2002).
- [30] J. Boronat, in *Microscopic Approaches to Quantum Liquids in Confined Geometries*, edited by E. Krotscheck and J. Navarro (World Scientific, Singapore, 2002), p. 21.
- [31] R. Jastrow, Many-body problem with strong forces, *Phys. Rev.* **98**, 1479 (1955).

- [32] L. Reatto and G. Chester, Phonons and the properties of a Bose system, *Phys. Rev.* **155**, 88 (1967).
- [33] H. T. Stoof, K. B. Gubbels, and D. Dickerscheid, *Ultracold Quantum Fields* (Springer, Berlin, 2009).
- [34] C. Chin, R. Grimm, P. Julienne, and E. Tiesinga, Feshbach resonances in ultracold gases, *Rev. Mod. Phys.* **82**, 1225 (2010).
- [35] G. F. Gribakin and V. V. Flambaum, Calculation of the scattering length in atomic collisions using the semiclassical approximation, *Phys. Rev. A* **48**, 546 (1993).
- [36] V. V. Flambaum, G. F. Gribakin, and C. Harabati, Analytical calculation of cold-atom scattering, *Phys. Rev. A* **59**, 1998 (1999).
- [37] J. L. Bohn, J. P. Burke, C. H. Greene, H. Wang, P. L. Gould, and W. C. Stwalley, Collisional properties of ultracold potassium: Consequences for degenerate Bose and Fermi gases, *Phys. Rev. A* **59**, 3660 (1999).
- [38] G. Thalhammer, G. Barontini, J. Catani, F. Rabatti, C. Weber, A. Simoni, F. Minardi, and M. Inguscio, Collisional and molecular spectroscopy in an ultracold Bose-Bose mixture, *New J. Phys.* **11**, 055044 (2009).
- [39] L. M. Jensen, H. M. Nilsen, and G. Watanabe, BCS-BEC crossover in atomic Fermi gases with a narrow resonance, *Phys. Rev. A* **74**, 043608 (2006).
- [40] S. Stringari and J. Treiner, Surface properties of liquid ^3He and ^4He : A density-functional approach, *Phys. Rev. B* **36**, 8369 (1987).
- [41] R. C. Tolman, The effect of droplet size on surface tension, *J. Chem. Phys.* **17**, 333 (1949).
- [42] E. Blokhuis and J. Kuipers, Thermodynamic expressions for the Tolman length, *J. Chem. Phys.* **124**, 074701 (2006).
- [43] P. Rehner and J. Gross, Surface tension of droplets and Tolman lengths of real substances and mixtures from density functional theory, *J. Chem. Phys.* **148**, 164703 (2018).
- [44] L. S. Bartell, Tolman's δ , surface curvature, compressibility effects, and the free energy of drops, *J. Phys. Chem. B* **105**, 11615 (2001).
- [45] S. Mayer, A molecular parameter relationship between surface tension and liquid compressibility, *J. Phys. Chem.* **67**, 2160 (1963).
- [46] W. Helfrich, Elastic properties of lipid bilayers: Theory and possible experiments, *Z. Naturforsch. C* **28**, 693 (1973).
- [47] S. Fisk and B. Widom, Structure and free energy of the interface between fluid phases in equilibrium near the critical point, *J. Chem. Phys.* **50**, 3219 (1969).
- [48] P. Egelstaff and B. Widom, Liquid surface tension near the triple point, *J. Chem. Phys.* **53**, 2667 (1970).
- [49] K. Mon and D. Stroud, Surface widths of simple liquids and an empirical law of freezing, *J. Chem. Phys.* **74**, 2078 (1981).
- [50] H. Hu and X.-J. Liu, Collective excitations of a spherical ultradilute quantum droplet, *Phys. Rev. A* **102**, 053303 (2020).